Results in Physics 22 (2021) 103940

Contents lists available at ScienceDirect

Results in Physics

journal homepage: www.elsevier.com/locate/rinp

Optical tomography dynamic for time-dependent coherent states generated by an open qubit-cavity system

A.-B.A. Mohamed [a,b,*], E.M. Khalil [c,d], M.M. Selim [a], H. Eleuch [e,f,g]

[a] Department of Mathematics, College of Science and Humanities in Al-Aflaj, Prince Sattam Bin Abdulaziz University, Saudi Arabia
[b] Faculty of Science, Assiut University, Assiut, Egypt
[c] Department of Mathematics, College of Science, P.O. Box11099, Taif University, Taif 21944, Saudi Arabia
[d] Faculty of Science Al-Azhar University, Nasr City, Cairo, Egypt
[e] Department of Applied Physics and Astronomy, University of Sharjah, United Arab Emirates
[f] Department of Applied Sciences and Mathematics, College of Arts and Sciences, Abu Dhabi University, Abu Dhabi 59911, United Arab Emirates
[g] Institute for Quantum Science and Engineering, Texas A&M University, College Station, TX 77843, USA

ARTICLE INFO

Keywords:
Optical tomography
Phase damping
Coherent states

ABSTRACT

Optical tomography is investigated for time-dependent quantum states, which are generated from coherent even and odd coherent cavity fields interacting with a two-level system (qubit) in the presence of phase damping. The effects of the qubit-cavity coupling, detuning, and cavity phase damping on the optical tomography distribution are studied. The dynamics of the optical tomography is explored for an open cavity field. We show an aspect of the alteration of the optical tomography distribution.

Introduction

The physical properties of quantum states (QSs) can be studied directly using the quantum state tomography (QST). This procedure determines an unknown QS based on a suitable measurement set [1]. The QST technique represents a monotonic relation between the quasiprobability and the field probability distributions [2], i.e., tomography is a probability representation of a quantum state. The goal of the optical tomography is to extract all possible information about the quantum states contained in the density operator. The optical tomography is a good indicator for the quantum effects [3–5] as: quantum correlations, coherence and phase space nonclasscality. Experimentally, QST is an essential tool for quantum information [6]. QST have been investigated theoretically and experimentally for spatial quantum states with a deformable mirror [6], linear optics and photon counting [7], excited coherent states associated to deformed oscillators [8], and dissipative nonlinear medium [9], nitrogen-vacancy center in diamond at room temperature [10].

Several experimental prototypes were proposed to realize qubit [11] as: superconducting circuits [12,13] quantum dot [14] trapped ions [15]. The interaction between a qubit and a cavity has been used to generate non-classical effects that are very useful to quantum information such as quantum correlations and non-classicality [16–20].

The interaction with the environment induces dissipation and decoherence which are the main responsible for the superposition vanishing [21–27]. One of the environment effects is the phase damping of an open cavity, which occurs when there is no energy exchange between the qubit-cavity system and the surrounding environment. It is closely related to decoherence phenomenon, where decoupling occurs on a time scale shorter than the energy dissipation [28,29].

In previous investigations of the optical tomography [30–32], the study on the effects of the qubit-cavity interactions on the optical tomography are limited to coherent states. In this work we explore the time-dependent optical tomography for coherent, even and odd coherent states in an open qubit-cavity system.

The paper is arranged as follows: In Section “The physical system” we describe the physical system. In Section “Tomographic representation of a mixed quantum state”, the tomographic representation of a quantum state density matrix is introduced. In Section “Optical tomography of the generated states via an open qubit-cavity system”, the results and discussion of the optical tomography of the generated time-dependent quantum states from an open qubit-cavity system are illustrated. Finally, the Section “Conclusions” is dedicated to the conclusion.

* Corresponding author at: Department of Mathematics, College of Science and Humanities in Al-Aflaj, Prince Sattam Bin Abdulaziz University, Saudi Arabia.
E-mail address: abdelbastm@aun.edu.eg (A.-B.A. Mohamed).

https://doi.org/10.1016/j.rinp.2021.103940
Received 25 November 2020; Received in revised form 1 February 2021; Accepted 1 February 2021
Available online 17 February 2021

The physical system

To generate time-dependent coherent field states, based on the initial superposition coherent states from an open qubit-cavity system, we consider an open coherent cavity field interacting with a qubit (with up $|\uparrow\rangle$ and down $|\downarrow\rangle$ states) and an energy-preserving reservoir. The qubit-cavity density matrix dynamic $\rho(t)$ in the presence of the phase cavity damping is given by

$$\frac{\partial}{\partial t}\widehat{\rho}\left(t\right) = -i\left[\widehat{H}, \widehat{\rho}\left(t\right)\right] + L\widehat{\rho}\left(t\right). \tag{1}$$

Under the rotating wave approximation, the qubit-cavity Hamiltonian $\widehat{H}$ is given by

$$\widehat{H} = \omega\widehat{a}^{\dagger}\widehat{a} + \omega_{\circ}\widehat{\sigma}_{z}\Big/2 + \lambda\left(\widehat{a}\sigma_{+} + \widehat{a}^{\dagger}\sigma_{-}\right), \tag{2}$$

where ω and $\omega_{\circ}$ are the cavity and the qubit frequencies, respectively, with the detuning $2\delta = \omega_{\circ} - \omega$, $\widehat{a}$ and $\widehat{a}^{\dagger}$ represent the cavity operators, λ designs the qubit-cavity coupling constant, and $\widehat{\sigma}_z$ and $\widehat{\sigma}_{\pm}$ are the qubit Pauli density matrices. The phase damping term $L\widehat{\rho}(t)$ that based on the photon number operator, $\widehat{N} = \widehat{a}^{\dagger}\widehat{a}$ is described by

$$L\widehat{\rho}(t) = \gamma([\widehat{a}^{\dagger}\widehat{a}\widehat{\rho}(t), \widehat{a}^{\dagger}\widehat{a}] + [\widehat{a}^{\dagger}\widehat{a}, \widehat{\rho}(t)\widehat{a}^{\dagger}\widehat{a}]), \tag{3}$$

with the decoherence coupling constant γ. In the high-Q cavity regime (the dephase damping rate γ is very small against the coupling λ), we can derive an analytical solution of Eq. (1) by using the eigenstates-Hamiltonian method [33–36]. The technique is based on the Hamiltonian eigenstates: For the spanned space of qubit-cavity states $\{|\uparrow, n\rangle, |\downarrow, n+1\rangle\}(n = 0, 1, 2, \ldots)$, the eigenstates $|D_n^{\pm}\rangle$ and the eigenvalues $E_n^{\pm}$ of the Hamiltonian $\widehat{H}$ are given by

$$\begin{aligned} |D_0\rangle &= \left|\downarrow, 0\right\rangle, \qquad E_0 = -\frac{\omega_{\circ}}{2}, \\ |D_n^{\pm}\rangle &= K_n^{\pm}|\uparrow, n\rangle \pm K_n^{\mp}|\downarrow, n+1\rangle, \end{aligned} \tag{4}$$

$$E_n^{\pm} = \omega\left(n + \frac{1}{2}\right) \pm \sqrt{\delta^2 + \lambda^2(n+1)}, \tag{5}$$

where

$$K_n^{\pm} = \frac{1}{\sqrt{2}}\sqrt{1 \pm \widetilde{\delta}_n}, \quad \widetilde{\delta} = \delta\Big/\pi_n, \pi_n = \sqrt{\delta^2 + \lambda^2(n+1)}. \tag{6}$$

Let us write the photon number operator $\widehat{N}$, which appears in Eq. (4) in terms of the matrices: $\widehat{M}_{11}^{n} = \left|D_n^{+}\rangle\langle D_n^{+}\right|$, $\widehat{M}_{12}^{n} = \left|D_n^{+}\rangle\langle D_n^{-}\right|$, $M_{21}^{n} = \left|D_n^{-}\rangle\langle D_n^{+}\right|$ and $\widehat{M}_{22}^{n} = \left|D_n^{-}\rangle\langle D_n^{-}\right|$ as,

$$\widehat{N} = \sum_{n=0}^{\infty}\left(n + K_n^{+2}\right)\widehat{M}_{11}^{n} - nK_n^{-}K_n^{+}\left(\widehat{M}_{12}^{n} + \widehat{M}_{21}^{n}\right) + \left(n + K_n^{-2}\right)\widehat{M}_{22}^{n}.$$

By using the canonical transformation,

$$\dot{W}\left(t\right) = e^{i\widehat{H}t}\frac{\partial\widehat{\rho}(t)}{\partial t}e^{-i\widehat{H}t} + i\left[\widehat{H}, W\left(t\right)\right],$$

the Eq. (1) takes the form

$$\begin{aligned} \dot{W}(t) = 2\gamma\sum_{j,k=0}^{\infty}&\left(f_j\widehat{M}_{11}^{j} + g_j\widehat{M}_{11}^{j}\right)W\left(f_k\widehat{M}_{11}^{k} + g_k\widehat{M}_{11}^{k}\right) + d_jd_k\left(\widehat{M}_{12}^{j}W\widehat{M}_{21}^{k}e^{2i\beta_{jk}t}\right. \\ &\left.+ \widehat{M}_{21}^{j}W\widehat{M}_{12}^{k}e^{-2i\beta_{jk}t}\right) - \gamma\sum_{j=0}^{\infty}\left(f_j^2 + h_j^2\right)\left(\widehat{M}_{11}^{j}W + W\widehat{M}_{11}^{j}\right) + \left(g_j^2\right. \\ &\left.+ h_j^2\right)\left(\widehat{M}_{22}^{j}W + W\widehat{M}_{22}^{j}\right), \end{aligned} \tag{7}$$

where $f_j = (j + K_j^{-2}), g_j = (j + K_j^{+2})$, $h_j = (K_j^{+}K_j^{-})$, and $\beta_{jk} = \pi_j - \pi_k$.

In order to find analytical solutions, we consider that the initial state of the system is given by

$$\begin{aligned} \rho(0) &= \sum_{m,n=0} P_mP_n\left|\uparrow, m\right\rangle\left\langle\uparrow, n\right| \\ &= \sum_{m,n=0} P_mP_n\left[K_m^{+}\left|D_m^{+}\right\rangle + K_m^{-}\left|D_m^{-}\right\rangle\right)\left(K_n^{+}\left|D_n^{+}\right\rangle + K_n^{-}\left|D_n^{-}\right\rangle\right], \end{aligned} \tag{8}$$

Note that the qubit is initially in the upper state $|\uparrow\rangle$. While the initial cavity field is considered to be a superposition of coherent states (SCS) that is defined as

$$\left|\alpha\right\rangle = \sum_{n=0}^{\infty}P_n\left|n\right\rangle, \tag{9}$$

P_n represents the photon number distribution of the SCS,

$$P_n = N\left[\frac{\alpha^n}{\sqrt{n!}} + r\frac{(-\alpha)^n}{\sqrt{n!}}\right]e^{-\frac{|\alpha|^2}{2}}, \tag{10}$$

where α represents the initial mean photon number operator, and r is the SCS parameter. The SCS can be reduced to coherent state with $r = 0$, even coherent state with $r = 1$, and odd coherent state with $r = -1$. The normalization factor has the following expression,

$$N^2 = \frac{1}{\left[1 + r^2 + 2r\exp\left(-2\left|\alpha\right|^2\right)\right]}. \tag{11}$$

By tracing the qubit states from the density matrix of the qubit-cavity system $\widehat{\rho}(t)$, the generated time-dependent state is given by

$$\begin{aligned} \widehat{\rho}^{f}(t) = \mathrm{Trace}_{qubit}\{\widehat{\rho}(t)\} = \sum_{m,n=0}&\left\{K_m^{+}K_n^{+}\Lambda_{mn}^{++}X_{m,n}^{+}\left(t\right) + K_m^{-}K_n^{-}\Lambda_{mn}^{--}X_{mn}^{-}\left(t\right)\right. \\ &\left.+K_m^{-}K_n^{+}\Lambda_{mn}^{-+}Y_{mn}^{-}\left(t\right) + K_n^{+}K_n^{-}\Lambda_{mn}^{+-}Y_{mn}^{+}\left(t\right)\right\}\left|m\right\rangle\left\langle n\right| + \left\{K_m^{-}K_n^{-}\Lambda_{mn}^{++}X_{m,n}^{+}\left(t\right)\right. \\ &\left.+ K_m^{+}K_n^{+}\Lambda_{mn}^{--}X_{mn}^{-}\left(t\right) - K_m^{+}K_n^{-}\Lambda_{mn}^{-+}Y_{mn}^{-}\left(t\right) - K_n^{-}K_n^{+}\Lambda_{mn}^{+-}Y_{mn}^{+}\left(t\right)\right\}\left|m\right. \\ &\left.+1\right\rangle\left\langle n+1\right|\Big], \end{aligned} \tag{12}$$

where $\Lambda_{mn}^{\pm\pm} = e^{-i(E_m^{\pm} - E_n^{\pm})t}$ and the coefficients $X_{mn}^{\pm}(t)$ and $Y_{mn}^{\pm}(t)$ are

$$X_{mn}^{\pm}\left(t\right) = \begin{cases} K_m^{\pm}K_n^{\pm}P_mP_ne^{-\gamma\left[\left(\Phi_m^{\pm} - \Phi_n^{\pm}\right)^2 + \Theta_m^2 + \Theta_n^2\right]t} & \forall\ m \neq n; \\ \frac{1}{2}P_nP_n\left(1 \pm \frac{\delta}{\mu_n}e^{-2\gamma\Theta_nt}\right) & \forall\ m = n. \end{cases} \tag{13}$$

where $\Phi_n^{\pm} = n + K_n^{\mp 2}, \Theta_n = K_n^{+}K_n^{-}$, and

$$Y_{mn}^{\pm}\left(t\right) = K_m^{\pm}K_n^{\mp}P_mP_ne^{-\gamma\left[\left(\Phi_m^{\pm} - \Phi_n^{\mp}\right)^2 + \Theta_m^2 + \Theta_n^2\right]t} \quad \forall m, n. \tag{14}$$

Based on the reduced cavity density matrix $\widehat{\rho}^{f}(t)$, the optical tomography dynamic of the generated field states will be discussed in the following section.

Tomographic representation of a mixed quantum state

The optical tomography for a quantum state represented by the density operator $\widehat{\rho} = |\psi\rangle\langle\psi|$ is defined as [30]:

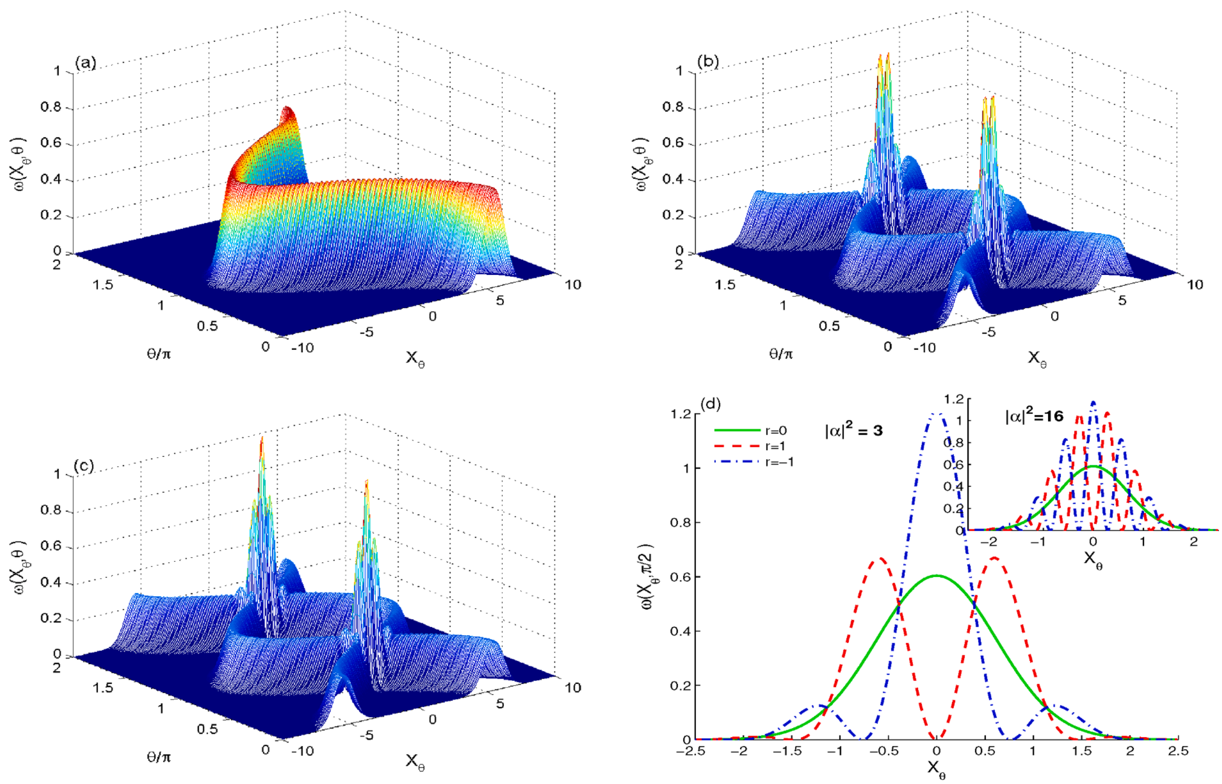

Fig. 1. Optical tomography, at $\lambda t=0$, of the cases: $r=0$ in (a), $r=1$ in (b) and $r=-1$ in (c) for $\theta\in[0,2\pi], X_\theta\in[-10,10]$ and $\left|\alpha\right|^2=16$. (d) shows $\omega\left(X_\theta,\theta=\frac{\pi}{2}\right)$ with different values of $\left|\alpha\right|^2$ at the fixed value $\theta=\frac{\pi}{2}$.

$$\omega\left(X_\theta,\theta\right)=\left\langle \widehat{X}_\theta|\widehat{\rho}|\widehat{X}_\theta\right\rangle, \tag{15}$$

where $\left|\widehat{X}_\theta\right\rangle$ represents the eigenstate of the homodyne quadrature operator

$$\widehat{X}_\theta=\frac{1}{\sqrt{2}}\left[\widehat{a}\exp\left(-i\theta\right)+\widehat{a}^\dagger\exp\left(i\theta\right)\right], \tag{16}$$

with eigenvalue X_θ and the local oscillator phase θ. $\widehat{a}$ and $\widehat{a}^\dagger$ represent the single-mode field operators. The above Eq. (15) satisfies the normalization condition,

$$\int\omega\left(X_\theta,\theta\right)dX_\theta=1. \tag{17}$$

After using the single-mode cavity field density matrix $\widehat{\rho}^f(t)$ of Eq. (12) into (15), the optical tomography formula is then

$$\omega\left(X_\theta,\theta,t\right)=\sum_{m,n=0}^{\infty}\rho^f_{mn}\left(t\right)\left\langle X_\theta,\theta|m\right\rangle\left\langle n|X_\theta,\theta\right\rangle, \tag{18}$$

where $\rho^f_{mn}(t)$ represent the elements of the matrix $\widehat{\rho}^f(t)$, and

$$\left\langle X_\theta,\theta|m\right\rangle=\frac{e^{-\frac{X_\theta^2}{2}}}{\pi^{\frac{1}{4}}}\frac{e^{-im\theta}H_m(X_\theta)}{\sqrt{m!2^m}},$$

$$\left\langle n|X_\theta,\theta\right\rangle=\frac{e^{-\frac{X_\theta^2}{2}}}{\pi^{\frac{1}{4}}}\frac{e^{in\theta}H_n(X_\theta)}{\sqrt{n!2^n}},$$

where $H_n(.)$ denotes the Hermite polynomial of order n. Eq. (18) sheds light on the temporal evolution of the optical tomography of a system containing the qubit-field interaction represented by the Eq. (2). In the

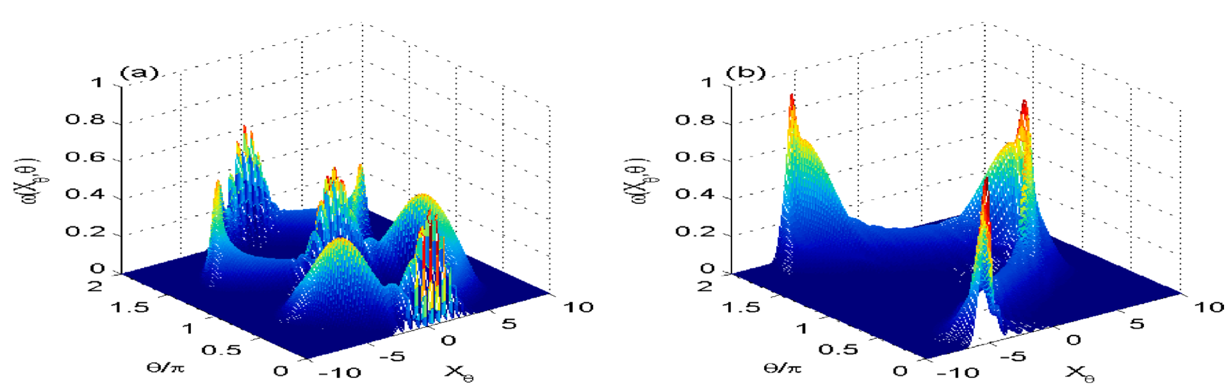

Fig. 2. Optical tomography of the generated coherent field cavity state for $r=0,\theta\in[0,2\pi],\left|\alpha\right|^2=16,\delta=0$ and $\gamma=0$ with different times: $\lambda t=\frac{1}{2}t_R$ in (a) and $\lambda t=t_R$ in (b).

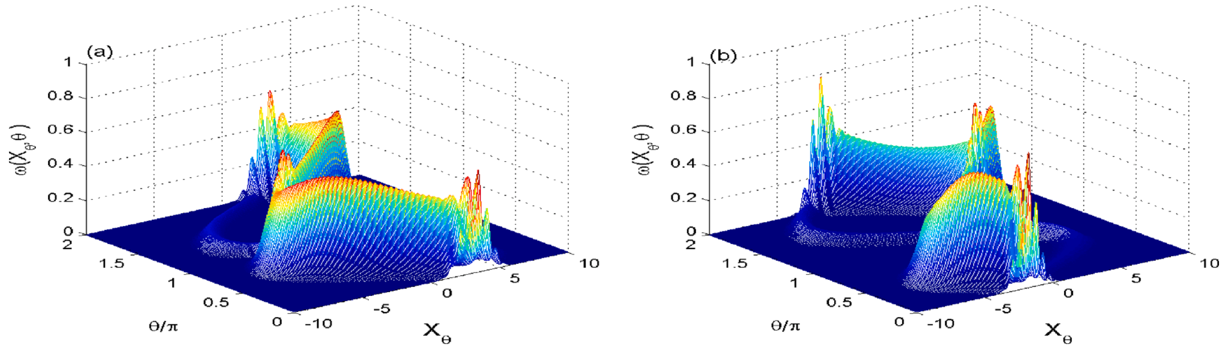

Fig. 3. The same of Fig. 2 but for the off-resonance case $\delta = 5\lambda$.

following sections we discuss the temporal evolution of the optical tomography for different types of initial states, namely coherent, even coherent, and odd coherent states in presence and absence of the phase damping.

Optical tomography of the generated states via an open qubit-cavity system

The time-dependent evolution of the optical tomography of the generated field states under the phase damping will be displayed. Fig. 1 shows the optical tomography $\omega(X_\theta, \theta, t = 0)$ of initial coherent, even coherent and odd coherent states. From Fig. 1(a), we observe that the optical tomography of the coherent state is a regular 2π-periodic sinusoidal function on θ. Its maximum value remains constant in the $\theta - X_\theta$ plane. The sinusoidal path of the optical tomography depends on the X_θ-parameter, it passes through the points $(X_\theta,\theta) = (|\alpha|^2\sqrt{2},0)$, $(X_\theta,\theta) = (-|\alpha|\sqrt{2},\pi)$, and then the point $(X_\theta,\theta) = (|\alpha|\sqrt{2},2\pi)$. Figs. 1(b) and (c) illustrate the optical tomography of the even $r = 1$ and odd $r = -1$ coherent states. The optical tomography of each of them is appeared as two regular sinusoidal paths, which are symmetric around $X_\theta = 0$ with π-period as a function of θ. This result completely agrees with the Eq. (17), since regular 2π-periodic sinusoidal function in the case $(r = 0)$ is divided into two identical paths in the cases $r = \pm 1$. The optical tomographies of the even and odd coherent states differ only at interference regions, which are centered at $\left(\theta, X_\theta\right) = \left(\frac{(2n+1)}{2}, 0\right)(n = 0, 1)$. Figs. 1(d) shows that this difference, between the optical tomography of the even and odd coherent states, depends on the initial coherent field intensity $|\alpha|^2 = 16$. It confirms that for the large field intensity values, the non-classicality of the even and odd coherent states are approximatively the same. At the fixed angle $\theta = \frac{\pi}{2}$, the optical tomography has a symmetric oscillatory dynamics with respect to $X_\theta = 0$. For $r = -1$, the maximum values of the optical tomography are larger than those of the case $r = 1$.

Fig. 2 illustrates the effect of the qubit-cavity interactions on the optical tomography of the coherent state for the resonance $\delta = 0$. At $t = \frac{1}{2}t_R$, the generated optical tomography $\omega(X_\theta, \theta, t)$ is a π-period function with respect to θ. It has two irregular sinusoidal paths, with respect to the axis $X_\theta = 0$, which are similar to shape optical tomography of the superposition of the coherent states $|\alpha\rangle$ and $|-\alpha\rangle$. This similarity can be

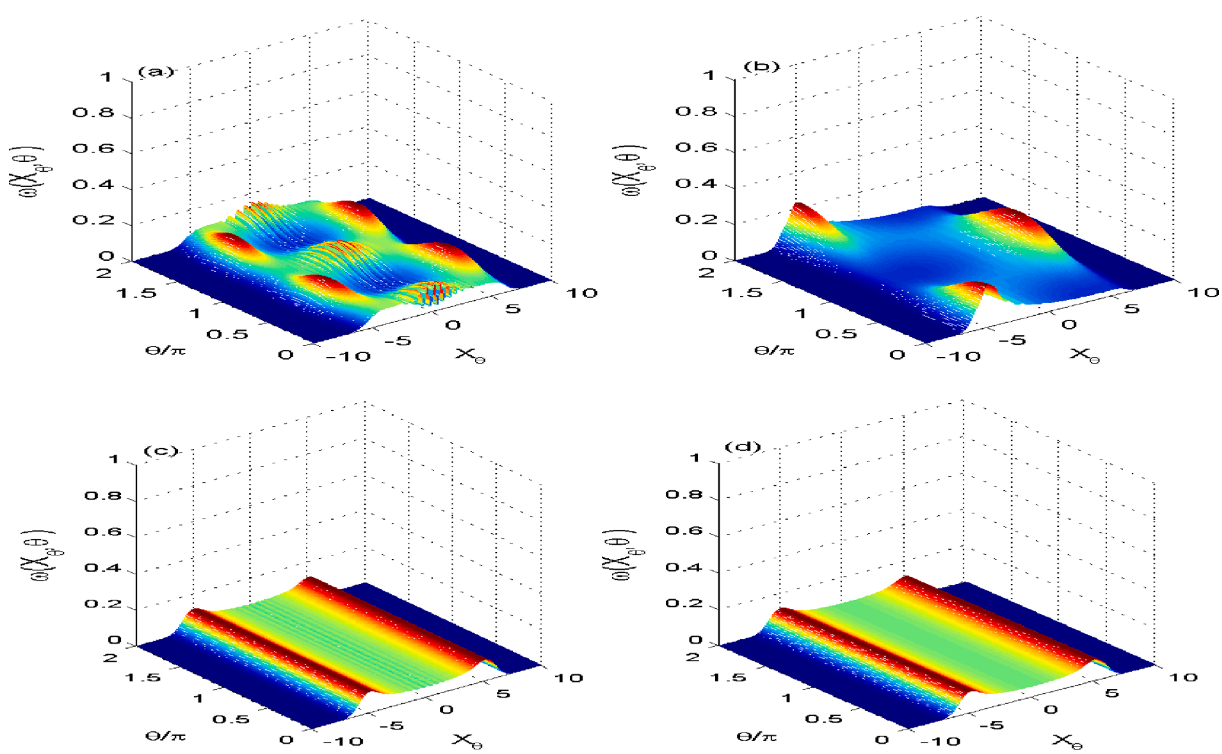

Fig. 4. The same of Fig. 2 but for $\gamma = 0.02\lambda$ in (a,b) and $\gamma = 0.2\lambda$ in (c,d).

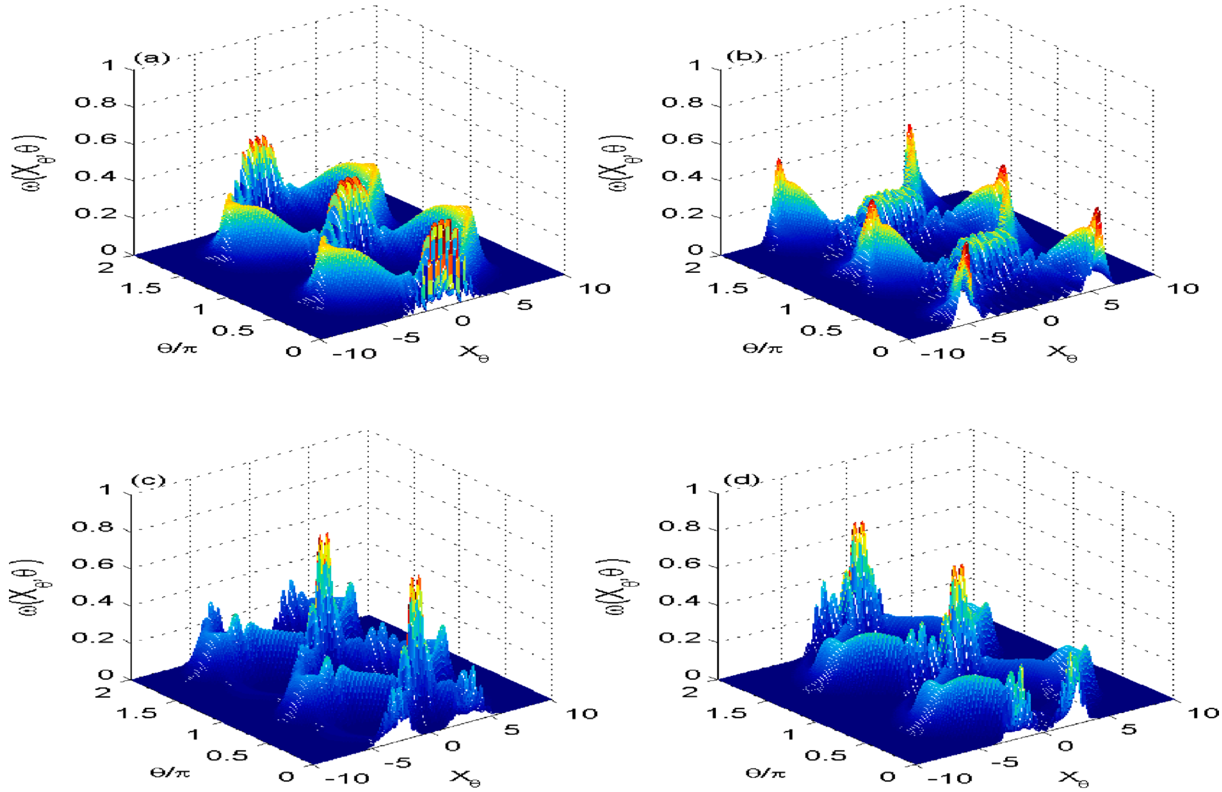

Fig. 5. Optical tomography for $r = 1, \theta \in [0, 2\pi], \left|\alpha\right|^2 = 16$ and $\gamma = 0$ at different times: $\lambda t = \frac{1}{2} t_R$ in (a) and $\lambda t = t_R$ in (b). With $\delta = 0$ in (a,b) and $\delta = 5\lambda$ in (c, d).

used as an indicator to the ability of the qubit-cavity interactions to generate the non-classicality or the quantum coherence in the qubit-cavity states. The function $\omega(X_\theta, \theta, t)$ has a maximum value at $\theta = 0$. It decreases and splits into two branches in two different paths as θ increases. It is followed by an increase until it reaches a maximum value at $\theta = \frac{\pi}{2}$, then a rise until it reaches the maximum value at $\theta = \pi$, see Fig. 2 (a). At the revival time $t = t_R$, the optical tomography is similar to that of the coherent state (see Fig. 1a) with different amplitudes and oscillations. The optical Tomography plot in Fig. 2(b) is similar to the one of Fig. 1a. This means that at the revival time $t = t_R$, the coherent cavity state has the same non-classicality as the initial optical tomography.

Fig. 3 displays the effect of the qubit-cavity detuning on the generated optical tomography. By comparing the Fig. 2 and Fig. 3, we find that the detuning affects the symmetry and regularity of the optical tomography. We observe that the qubit-cavity detuning affects the maximum values of the optical tomography as well as the shape distribution. The qubit-cavity detuning leads to an another nonclassicality.

Fig. 4, illustrates the effect of the cavity phase damping with different values $\gamma = 0.02\lambda$ and $\gamma = 0.2\lambda$. With this effect, the optical tomography maximum gradually decreases until it is completely wiped out. For small value of the phase damping, the irregular sinusoidal paths and distribution amplitudes of the optical tomography are reduced. From Fig. 4(c,d), we observe that the increase of the cavity phase damping leads to the vanishing of the sinusoidal distribution. The generated optical tomography is distributed between the two axes $X_\theta = \pm 4\sqrt{2}$.

Fig. 5 shows the optical tomography for the field states at different times when the cavity field is initially in the even coherent state. For the resonance case $\delta = 0$ and $\lambda t = \frac{1}{2} t_R$ (see Fig. 5a), the symmetry and regularity of the optical tomography sinusoidal paths are pronounced, and are less than those of the initial even coherent state. The qubit-cavity interactions reduce the oscillation amplitudes of the initial optical tomography distributions. At $\lambda t = t_R$ (see Fig. 5b), the qubit-cavity interactions increase the interfered buttons and picks of the initial optical tomography. The generated interfered distributions of the optical tomography is due to the non-classicality of the even coherent state which

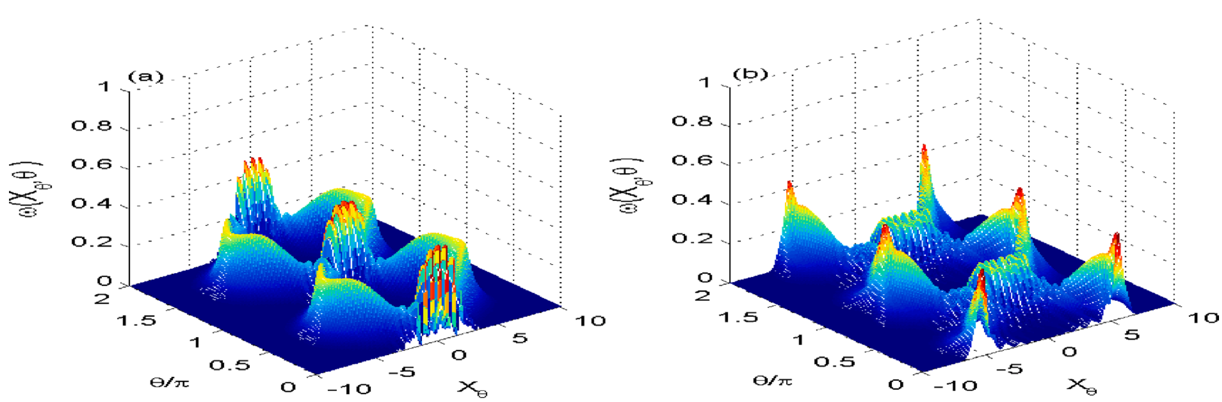

Fig. 6. The same of Fig. 5 but for the initial odd coherent. state $r = -1$.

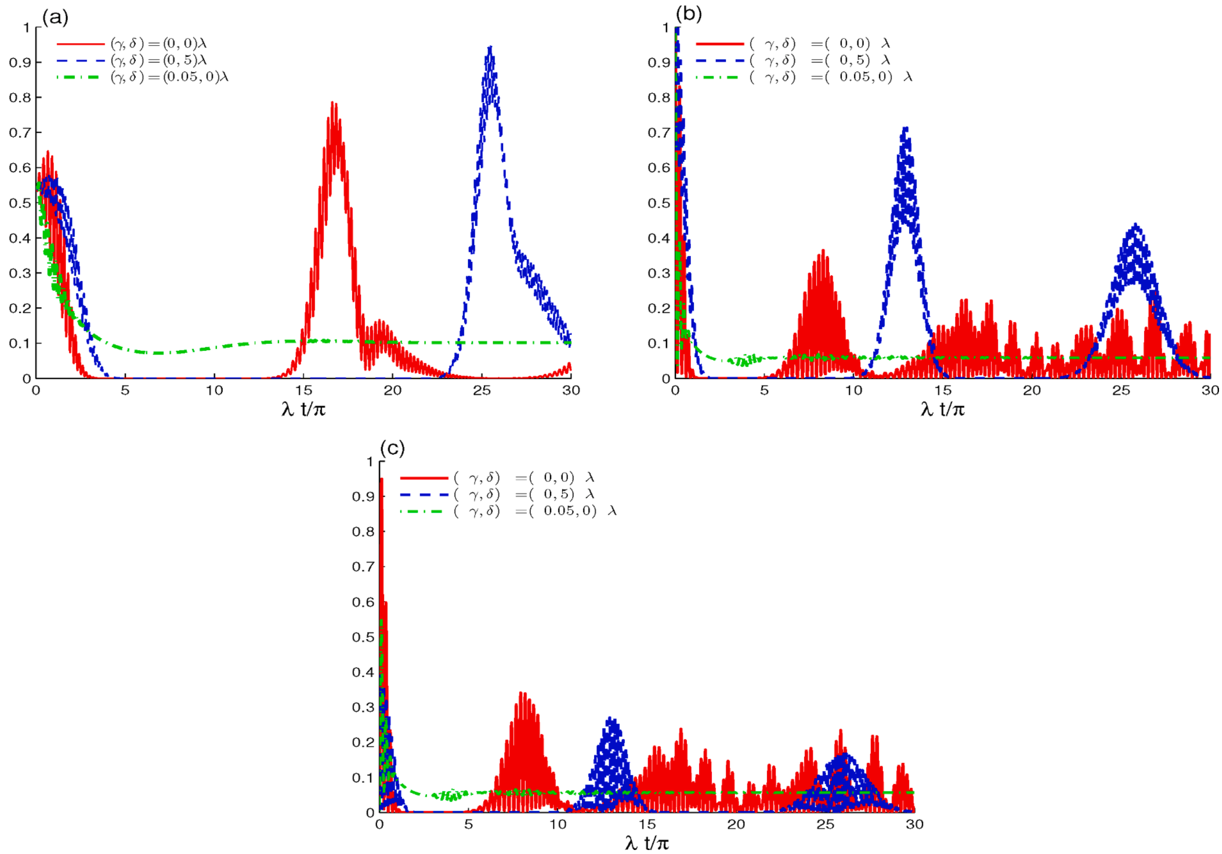

Fig. 7. The dynamics of the maximum value of the optical tomography $\omega_{\max}(-5.5,\pi,t)$ for the case $r=0$ in (a) and $\omega_{\max}(0.3,1.5\pi,t)$ for the cases $r=1$ in (b) and $r=-1$ in (c) with different values for δ and γ at $|\alpha|^2=16$.

is larger than the one of the coherent state.

The plots of the Figs. 5c and 5d illustrate the effect of the qubit-cavity detuning on the optical tomography distributions for the case $r=1$. The results confirm that the detuning affects the symmetry and regularity of the optical tomography. The detuning leads to the change of the amplitudes, frequency, and shapes of the optical tomography. From Fig. 6, we deduce that the generated optical tomography when the cavity field is initially in the odd coherent state $r=-1$ is similar to the case of even coherent state $r=1$. This confirm that, for large field intensity values $|\alpha|^2=16$, the non-classicality of the even and odd coherent states are approximatively the same.

Fig. 7 illustrates the dynamics of the maxima of the optical tomography for the cases $r=0$ and $r=\pm1$. For $r=0$, the maximum value of the optical tomography $\omega_{\max}(-5.5,\pi,t)$ is determined from Fig. 1a. While for the cases $r=\pm1$, $\omega_{\max}(0.3,1.5\pi,t)$ is chosen from Fig. 1b,c. For the coherent state (see Fig. 7a), the optical tomography $\omega_{\max}(-5.5,\pi,t)$ starts from its maximum value, oscillates and collapses for a large time interval. After this collapse/disappearance interval, the optical tomography increases, as can be seen in the Fig. 7a. The collapse interval and the maximum values of the optical tomography are increased for the non-resonance case. Dash-dot curve shows that, after a short period of time, the generated optical tomography decays to reach its non-zero stationary value $\omega_{\max}(0.3,1.5\pi,\infty)\approx0.1$.

Fig. 7b is plotted for the even coherent state case. We find that the oscillations of the distribution $\omega_{\max}(0.3,1.5\pi,t)$ have small amplitudes and large frequencies compared to those of the coherent case. The qubit-cavity detuning $\delta=5\lambda$ leads slightly to the rise of the optical tomography distribution. Consequently the periods of collapse increase. Dash-dot curve illustrates the cavity phase damping effect on the optical tomography distribution.

Fig. 7c shows the dynamics of the optical tomography $\omega_{\max}(0.3,1.5\pi,t)$ for the case of the odd coherent state under the effects of the qubit-cavity detuning and the cavity phase damping. We find that the amplitudes, frequency, and stationary value of the generated optical tomography oscillations depend on the detuning and the dephasing. They differ from those of the case of the even coherent state.

Conclusions

In this paper, we have studied the time-dependent evolution of the optical tomography of an open coherent cavity field interacting with a qubit system. The energy-preserving reservoir coupling that leads to cavity phase damping is considered. The effect of the qubit-cavity coupling, qubit-cavity detuning, and cavity phase damping on the optical tomography distribution is studied for the cavity field in the coherent, even and odd coherent states. It is found that the regularity and the symmetry of the optical tomography distributions are more pronounced with the detuning in the case of the even and odd coherent states. The amplitude, frequency, and stationary value of the generated optical tomography oscillations are very sensitive to the initial cavity field, detuning and the phase damping.

Declaration of Competing Interest

The authors declare that they have no known competing financial interests or personal relationships that could have appeared to influence the work reported in this paper.

Acknowledgments

The authors are very grateful to the referees and the editor for their constructive remarks, which have helped to improve the manuscript. Taif University Researchers Supporting Project number (TURSP-2020/17), Taif University, Taif, Saudi Arabia.

References

[1] Leonhardt U. Measuring the Quantum State of Light. Cambridge: Cambridge University Press; 1997.
[2] Vogel K, Risken H. Phys Rev A 1989;40:2847.
[3] Mohamed A-BA, Eleuch H. Sci Rep 2020;10:13240.
[4] Mohamed A-BA, Eleuch H, Raymond Ooi CH, Sci. Rep. 9, (2019) 19632; and in Phys. Lett. A 383, (2019) 125905.
[5] Hessian HA, Mohamed A-BA. Laser Phys 2008;18:1217.
[6] Kravtsov KS, Zhutov AK, Kulik SP. Phys Rev A 2020;102:023706.
[7] Banchi L, Kolthammer WS, Kim MS. Phys Rev Lett 2018;121:250402.
[8] Almarashia AM, Algarnia A, Alabouda FM, Abdel-Khalekb S, Berrada K, Results Phys 14, (2019) 102352.
[9] Rohith M, Sudheesh C. Phys Rev A 2015;92:053828.
[10] Chen B, Geng J, Zhou F, Song L, Shen H, Xu N. Appl Phys Lett 2019;114:041102.
[11] Armenta Rico RJ, Maldonado-Villamizar FH, Rodriguez-Lara BM. Phys Rev A 2020;101:063825.
[12] Wallraff A, Schuster DI, Blais A, Frunzio L, Huang R-S, Majer J, Kumar S, Girvin SM, Schoelkopf RJ. Nature 2004;431:162.
[13] Felicetti S, Rossatto DZ, Rico E, Solano E, Forn- Díaz P. Phys Rev A 2018;97:013851.
[14] Stufler S, Machnikowski P, Ester P, Bichler M, Axt VM, Kuhn T, Zrenner A. Phys Rev B 2006:125304.
[15] Puebla R, Hwang M-J, Casanova J, Plenio MB. Phys Rev A 2017;95:063844.
[16] Nielsen MA, Chuang IL. Quantum Computation and Quantum Information. Cambridge: Cambridge University Press; 2000.
[17] Obada A-SF, Hessian HA, Mohamed A-BA, Homid AH. J Opt Soc Am B 2013;30:1178.
[18] Obada A-SF, Hessian HA, Mohamed A-BA, Homid AH. Quantum Inf Process 2014;13:475.
[19] Mohamed A-BA, Eleuch H. J Opt Soc Am B 2018;35:47.
[20] Obada A-SF, Mohamed A-BA. Opt Commun 2013;309:236.
[21] Ban M. Phys Lett A 2021;385:126936.
[22] Abdel-Aty A-H, Kadry H, Mohamed ABA, Eleuch H. Sci Rep 2020;10:16640.
[23] Xie Y-X, Qin Z-Y. Quantum Inf Process 2020;19:375.
[24] Mohamed A-BA, Eleuch H. Eur Phys J Plus 2017;132:75.
[25] Mohamed A-BA. Eur Phys J D 2017;71:261.
[26] Mancini S, Bonifacio R. Phys Rev A 2001;63:032310.
[27] Mohamed A-BA. Phys Lett A 2010;374:4115.
[28] Palma GM, Suominen K-A, Ekert AK, Proc R Soc London, Ser A 452, (1996) 567.
[29] Obada A-SF, Mohamed A-BA. Opt Commun 2012;285:3027.
[30] Korennoy YA, Man'ko VI. Phys Rev A 2011;83:053817.
[31] Filippov SN, Man'ko VI. Phys Scr 2011;83:058101.
[32] Miranowicz A, Paprzycka M, Pathak A, Nori F. Phys Rev A 2014;89:033812.
[33] Puri RR, Agarwal GS. Phys Rev A 1987;35:3433.
[34] Obada A-SF, Hessian HA, Mohamed A-BA. J Phys B 2007;40:2241.
[35] Abdalla MS, Obada AS-F, Khalil EM, Mohamed A-BA. Solid State Commun 2014;184:56.
[36] Mohamed A-BA, Farouk A, Yassen MF, Eleuch H. Appl Sci 2020;10:3782.